PV integration in curved parts: mechanical limits and key parameters from a theoretical point of view

Jean-Baptiste Charpentier, Tatiana Duigou, Bertrand Chambion, Philippe Voarino, Fabien Chabuel

Received: 30 June 2022 | Revised: 9 November 2022 | Accepted: 19 December 2022

DOI: 10.1002/pip.3666

SPECIAL ISSUE ARTICLE

PROGRESS IN PHOTOVOLTAICS WILEY

Photovoltaic integration in curved parts: Mechanical limits and key parameters from a theoretical point of view

Jean-Baptiste Charpentier | Tatiana Duigou | Bertrand Chambion | Philippe Voarino | Fabien Chabuel

Univ Grenoble Alpes, CEA-LITEN, INES, Le Bourget-du-Lac, France

Correspondence
Jean-Baptiste Charpentier, Univ Grenoble Alpes, CEA-LITEN, INES, 50 avenue du Lac Léeman, 73375 Le Bourget-du-Lac, France.
Email: jean-baptiste.charpentier@cea.fr

Funding information
Association Instituts Carnot

Abstract

Photovoltaic cells are produced as thin flat layers. They behave as a brittle and elastic material that fails at a given level of stress. Conforming cells into curved geometries will a priori induce both flexure and membrane stresses. In the present work, an analytical model is derived to predict both stress distributions and intensities in a mono-crystalline pseudo-square cell. Furthermore, a second model is derived to find the main stresses within fractions of cells. For conventional cell dimensions, solutions predict a transition from flexure to membrane dominated stresses for most conformations as curvature increases. As a consequence, near failure stresses are mainly determined by cells size and aspect ratio. In contrast, flexion is the main contribution in a small subset of the curvature space or for small curvatures. In the corresponding cases, stresses scale in proportion to cells thickness. As a consequence, cell size and/or shape is the main parameter to reduce internal stresses in most cases. In particular, the use of fractions of cells can substantially decrease membrane stresses and thus increase the maximum curvature. For instance, in a case study with M0 cells and curvature radii of a few meters, the highest predicted tensile stress is 45 MPa. In such a case, the larger M12 format gives a prediction of 65MPa. In contrast, thirds of cells give predictions of 25 and 30MPa, respectively.

KEYWORDS
BIPV, mechanics, module design, VIPV

1 | INTRODUCTION

In recent years, the growth of photovoltaics (PV) led to its introduction in new industrial fields. In some of the corresponding applications, surfaces exposed to sunlight are shaped by unyielding constraints. In contrast, standard mono-crystalline silicon PV cells are produced as thin flat pseudo-squares. In conventional modules, these cells are embedded into a thin and soft layer of polymer, that is, the encapsulant. This assembly lies between two protective layers, at least one of which being stiff and thick such that it defines the module shape. As a consequence, the central layer is strongly constrained. Without any specific solutions, the integration of cells in a curved structure will cause their conformation to the local shape of the stiff layer.

From a mechanical point of view, cells behave as mono- or poly-crystalline silicon,[1] which both are elastic and brittle. Owing to their elastic behavior, there is a simple relation between strains and stresses. Due to their brittle nature, the level of stress at which they fail is mostly defined by their toughness and the size and orientation of pre-existing defaults. These defaults are mainly located near cells surfaces and take the form of micro-grooves of a few tens of microns, which come as a consequence of the sawing process.[2–5] The characteristics and impacts of these defaults are therefore strongly influenced by the surface treatments performed afterwards.[6,7] Regarding crack

propagation, the local orientation of the crystalline structure has a noticeable influence on its fracture toughness.[6,8] In addition, the type and direction of the mechanical loading impact it as well.[4,9] These effects explain the wide scattering of characteristic fracture stress values (80–300 MPa) assessed and reported in the literature.[4,6,7,9–12] Furthermore, these experiments are expected to be scattered themselves since failure depends on a statistical event (the interaction between a stress field and the pre-existing cracks). Therefore, the characteristic fracture stress of a type of PV cell is not specific to every single cell of this type. However, the key failure metric will be the stress distribution within the cells and the characteristic fracture stress is a relevant quantity to predict mechanical failure statistically.

Considering a given cell in a curved module, both flexure and membrane strains are expected. These two contributions are independant of each other. On the one hand, curving a thin layer induces a gradient of lengths throughout the cell thickness at a given in-plane position. As a consequence, a strain gradient exists throughout the layer. The corresponding strains scale linearly with the system thickness and the local curvature regardless of the system in-plane size and shape. This first contribution is the flexure one. On the other hand, complex curvatures induce inconsistent in-plane changes of lengths. These changes generate strain fields constant throughout the system thickness but variable in the system plane. The corresponding strain field depends on the system in-plane size and shape and it grows with the Gaussian curvature.[13,14] This second contribution is the membrane one. Thus, the co-existence of both effects leads to non-trivial relations between the problem input parameters and the output stress distributions within cells.

From a mechanical designer point of view, stresses must be predicted for a given design and a certain criterion, function of the stress field, should be fulfilled to ensure cells integrity. The conventional approach is to use a numerical method to predict the stress field in classical PV applications[15–17] and other problems which require to curve silicon wafers.[18,19] Depending on the outcome, a wider parameter space exploration may be required to find a satisfactory design through an automated or a manual process. The main advantage of this method is its ability to find a solution for nonlinear and/or complex mechanical problems (including a large number of parameters). However, its main drawback is to provide little to no insight on the physics behind it. An alternative approach is to seek for the solution of a simple but representative analytical problem. The analytical solution of this problem provides the algebraic functions behind each value. As a consequence, the relative influence of each parameter is intelligible. This second approach, when achievable, provides clear answers and paths for design optimization.

In the present work, a model is derived to predict membrane stresses in a flat pseudo-square mono-crystalline cell conformed to a constant but anisotropic curvature. From this point, the problem is segmented into three simpler problems through a first-order approximation. The main problem derivation and segmentation are presented in Section 2. Model predictions are reported in Section 3 and confronted to finite element models (FEM) simulations. Finally, the practical implications of these results are discussed in Section 4.

2 | THEORY AND DERIVATION

2.1 | Kinematics

In order to find the membrane contribution, a flat and infinitely thin elastic layer (Ω) is considered. At every point $\underline{X}$ within this layer, the Green–Lagrange strain tensor $\underline{\underline{\epsilon}}$ writes

$$\underline{\underline{\epsilon}} = \frac{1}{2}\left({}^{t}\underline{\underline{\nabla}}\underline{u} + \underline{\underline{\nabla}}\underline{u} + {}^{t}\underline{\underline{\nabla}}\underline{u}.\underline{\underline{\nabla}}\underline{u}\right) \tag{1}$$

with $\underline{\underline{\nabla}}$ the gradient operator, $\underline{u}$ the displacement vector, and ${}^{t}\underline{a}$ the transpose of $\underline{a}$. In the following, vectors and tensors are separated in their in-plane and out-of-plane components. The layer conformation to a given shape is modeled through an imposed out-of-plane displacement $u_z\underline{e}_z$ with $\underline{e}_z$ perpendicular to the initial layer plane. Such a displacement produces an in-plane strain tensor $\underline{\underline{\epsilon}}^{\kappa}$ according to the non-linear term of Equation (1):

$$\underline{\underline{\epsilon}}^{\kappa} = \frac{1}{2}\begin{bmatrix} \left(\frac{\partial u_z}{\partial r}\right)^2 & \frac{1}{r}\frac{\partial u_z}{\partial \theta}\frac{\partial u_z}{\partial r} \\ \frac{1}{r}\frac{\partial u_z}{\partial \theta}\frac{\partial u_z}{\partial r} & \frac{1}{r^2}\left(\frac{\partial u_z}{\partial \theta}\right)^2 \end{bmatrix} \tag{2}$$

in a polar coordinate system. In the following, the imposed curvature κ is assumed to be small at the system scale R, $1 \ll \kappa R$. Silicon fails at minute levels of strain ($\sim 10^{-3}$). Thus, regarding the in-plane strains generated by in-plane displacements, second order strain terms are negligible and neglected. Therefore, according to Equation (1) this strain component $\underline{\underline{\epsilon}}^{p}$ writes

$$\underline{\underline{\epsilon}}^{p} = \begin{bmatrix} \frac{\partial u_r}{\partial r} & \frac{1}{2}\left(\frac{\partial u_\theta}{\partial r} - \frac{u_\theta}{r} + \frac{1}{r}\frac{\partial u_r}{\partial \theta}\right) \\ \frac{1}{2}\left(\frac{\partial u_\theta}{\partial r} - \frac{u_\theta}{r} + \frac{1}{r}\frac{\partial u_r}{\partial \theta}\right) & \frac{1}{r}\left(\frac{\partial u_\theta}{\partial \theta} + u_r\right) \end{bmatrix} \tag{3}$$

with u_r and u_θ the in-plane displacement components. In small strains, the total strain tensor $\underline{\underline{\epsilon}}$ is the sum of each contribution.

$$\underline{\underline{\epsilon}} = \underline{\underline{\epsilon}}^{p} + \underline{\underline{\epsilon}}^{\kappa} \tag{4}$$

Since silicon is elastic, the total strain tensor is equal to the elastic strain one. The normal displacement u_z can be expressed as a power series in a cartesian basis. It describes the system conformation to a regular shape. In this power series, the lowest order terms are expected to be the leading ones thanks to the small curvature hypothesis. In the present mechanical problem terms of orders 0 and 1 correspond to pure translations and rotations, respectively. Therefore, the first terms that cause strains are of second order. Higher order terms of the expansion are neglected. For a regular displacement u_z, the second order terms are related to the Hessian matrix of u_z. Due to the symmetry of this matrix, there will always be two eigen curvatures κ_1 and κ_2 and a phase shift ϕ_k such that u_z writes

$$u_z(r,\theta)=\frac{r^2}{4}\left((\kappa_\Sigma+\kappa_\Delta)\cos^2(\theta-\phi_k)+(\kappa_\Sigma-\kappa_\Delta)\sin^2(\theta-\phi_k)\right) \quad (5)$$

where $\kappa_\Sigma=\kappa_1+\kappa_2$ and $\kappa_\Delta=\kappa_1-\kappa_2$. For matter of illustration, the case $\kappa_\Sigma\neq 0$, $\kappa_\Delta=0$ corresponds to the mapping of the system on a sphere and the case $\kappa_\Sigma=0$, $\kappa_\Delta\neq 0$ to the mapping of the system on a saddle. Please note that according to Equation (5), both curvatures are assumed constant at the system scale. Using Equations (2) and (5), $\underline{\underline{\epsilon}}^\kappa$ writes

$$\underline{\underline{\epsilon}}^\kappa(r,\theta+\phi_k)=\frac{r^2}{8}\begin{bmatrix}\kappa_\Sigma^2+\frac{\kappa_\Delta^2}{2}+2\kappa_\Sigma\kappa_\Delta\cos(2\theta)+\frac{\kappa_\Delta^2}{2}\cos(4\theta) & -\kappa_\Delta\kappa_\Sigma\sin(2\theta)-\frac{\kappa_\Delta^2}{2}\sin(4\theta)\\ -\kappa_\Delta\kappa_\Sigma\sin(2\theta)-\frac{\kappa_\Delta^2}{2}\sin(4\theta) & \frac{\kappa_\Delta^2}{2}(1-\cos(4\theta))\end{bmatrix} \quad (6)$$

However, according to Equation (4), $\underline{\underline{\epsilon}}^\kappa$ will cause strains only if its three independent terms cannot be canceled by a remarkable displacement. As shown in Appendix A.1, $\underline{\underline{\epsilon}}^\kappa$ terms of spatial frequencies 2 and 4 can be canceled and the remaining one can be expressed in another fashion. With these modifications, the effective component of $\underline{\underline{\epsilon}}^\kappa$ writes

$$\underline{\underline{\epsilon}}^\kappa(r,\theta)=\frac{r^2}{8}\begin{bmatrix}\kappa_\Sigma^2-\kappa_\Delta^2 & 0\\ 0 & 0\end{bmatrix} \quad (7)$$

This result implies that the spatial orientation of the curvature, that is, ϕ_k, has no impact on membrane strains. Its unique curvature term $\kappa_\Sigma^2-\kappa_\Delta^2=4\kappa_1\kappa_2$ hides the Gaussian curvature. Furthermore, the remaining terms can be canceled if and only if $\kappa_\Sigma^2=\kappa_\Delta^2$, that is, in pure flexion cases. Therefore, and thanks to the linearity of Equations (3) and (4) and with no other loading on the system, the solution with $\kappa_\Sigma=\kappa$, $\kappa_\Delta=0$ is exactly the opposite of the solution for a problem of curvatures $\kappa_\Sigma=0$, $\kappa_\Delta=\kappa$ for every value of κ (see Appendix A.1). Please note that these results remain valid regardless of the system behavior isotropy/anisotropy or shape. Thus far, the system thickness was nil. As a consequence, the strain tensor $\underline{\underline{\epsilon}}$ only describes the membrane strain. Now, considering a system with a finite thickness W, a new contribution arises: flexure. The corresponding strains are maximum in the vicinity of both faces of the system. In the present framework, the flexure strain tensor writes

$$\underline{\underline{\epsilon}}^f(r,\theta)=\pm\frac{W}{4}\begin{bmatrix}\kappa_\Sigma+\kappa_\Delta\cos(2(\theta-\phi_k)) & -\kappa_\Delta\sin(2(\theta-\phi_k))\\ -\kappa_\Delta\sin(2(\theta-\phi_k)) & \kappa_\Sigma-\kappa_\Delta\cos(2(\theta-\phi_k))\end{bmatrix} \quad (8)$$

and the sign in Equation (8) depends on the considered face. The total strain at a given position is the sum of $\underline{\underline{\epsilon}}^f$ and $\underline{\underline{\epsilon}}$. Please note that Equation (8) gives an explicit prediction for the flexure term $\underline{\underline{\epsilon}}^f$. However, there is no explicit prediction for the membrane term $\underline{\underline{\epsilon}}$ yet since the in-plane strain tensor $\underline{\underline{\epsilon}}^p$ remains to be found. An explicit expression is looked for in the upcoming sections.

2.2 | Problem closure

Depending on its microstructure, silicon behaves as an isotropic or a cubic elastic material.[1] In both cases, there is a simple linear relation between strains and stresses and its plane-stress behavior writes

$$\underline{\underline{\sigma}}(\theta)=\frac{E}{1-\nu^2}\left(\begin{bmatrix}1 & \nu & 0\\ \nu & 1 & 0\\ 0 & 0 & \frac{1-\nu}{2}\end{bmatrix}+b\begin{bmatrix}f(\theta) & -f(\theta) & g(\theta)\\ -f(\theta) & f(\theta) & -g(\theta)\\ g(\theta) & -g(\theta) & 1-f(\theta)\end{bmatrix}\right).\underline{\underline{\epsilon}} \quad (9)$$

with E and ν silicon Young's modulus and Poisson's coefficient. b is an anisotropy factor, the behavior is isotropic if $b=0$ and anisotropic (cubic) otherwise. The purely isotropic tensor will be referred to as $\underline{\underline{C}}^i$ in the following. The anisotropic tensor $\underline{\underline{C}}^\mu$ relies on $f(\theta)=(1-\cos(4\theta))/2$ and $g(\theta)=\sin(4\theta)$. It is obtained through the rotation of the cubic tensor. Please note that the polar basis is assumed to be oriented in the <100> direction ($\theta=0$). Mono-crystalline silicon corresponds to $b=0.21$ (using values from Hall[20]). Finally, $\underline{\underline{\sigma}}$ and $\underline{\underline{\epsilon}}$ are defined using Voigt's notation. Regarding the mechanical equilibrium, without any external loading or additional constraint, it writes

$$\underline{\nabla}.\left(\underline{\underline{\sigma}}\right)=\underline{0} \quad (10)$$

with $\underline{\nabla}$ the divergence operator. Furthermore, the boundary conditions writes

$$\underline{\underline{\sigma}}.\underline{n}=\underline{0}\ (\partial\Omega) \quad (11)$$

where $\underline{n}$ is the vector normal to the outer boundary. The relevance of this assumption, that is, no external loading or additional constraint, is discussed in Section 4. Thus far, the system shape remains undefined. In the following, the outer boundary will be described as

$$R(\theta)=R_0+R_0\sum_{n=1}^{N}c_n\cos(n\theta) \quad (12)$$

where the coefficients c_n can be chosen to match a broad set of shapes, which includes the pseudo-square. The derivation of c_n values is presented in Appendix A.1.1 for a pseudo-square shape. Their values and the corresponding shape are presented in Figure 1.

To summarize, the present problem (E) seeks for the in-plane displacement field $\underline{u}$ such that

$$\begin{array}{ll}(\Omega) & \left|\begin{array}{l}\underline{\underline{\epsilon}}^\kappa(r)=\left(\kappa_\Sigma^2-\kappa_\Delta^2\right)\frac{r^2}{8}\begin{bmatrix}1 & 0\\ 0 & 0\end{bmatrix}\\ \underline{\underline{\sigma}}=\underline{\underline{C}}:\left(\frac{1}{2}\left({}^t\underline{\nabla}\underline{u}+\underline{\nabla}\underline{u}\right)+\underline{\underline{\epsilon}}^\kappa\right)\\ \underline{\nabla}.\left(\underline{\underline{\sigma}}\right)=\underline{0}\end{array}\right.\\ (\partial\Omega) & \left|\underline{\underline{\sigma}}.\underline{n}=\underline{0}\right.\end{array} \quad (E)$$

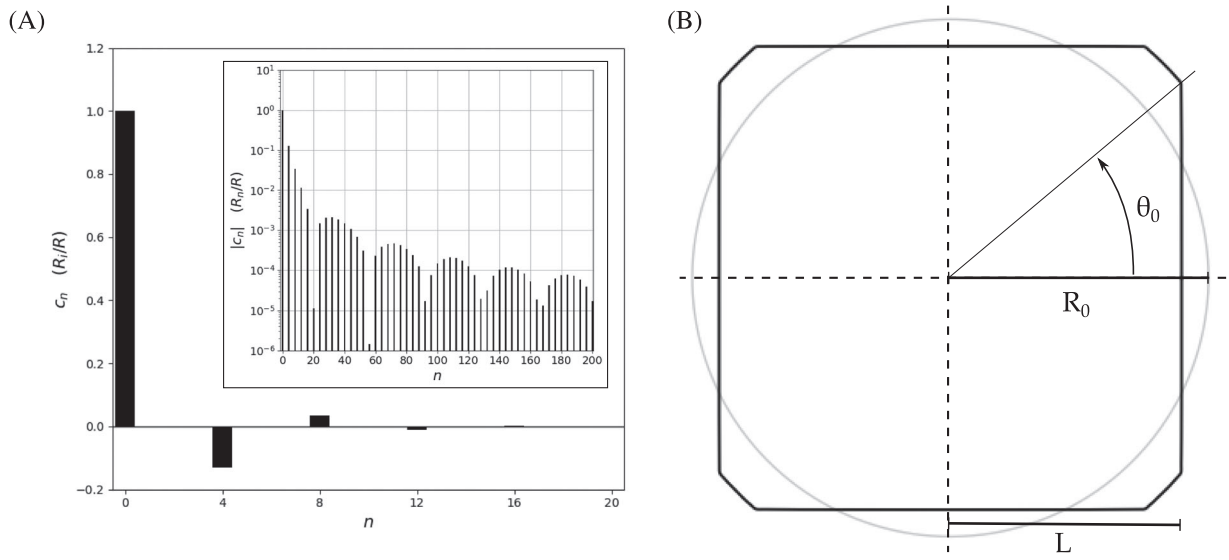

FIGURE 1 (A) Values of the 20 first coefficients c_n for a pseudo-square shape. (B) Shape of the pseudo-square computed with the Fourier series coefficients

In the above set of equations, is the double dot product. The solution to this problem gives the strains (through Equations 3 and 4) and stresses (with Equation 9).

2.3 | Problem segmentations

The problem (E) is not trivial. The two main sources of complexity arise from the anisotropic material behavior and the pseudo-square shape. However, one can notice that the dimensionless anisotropic parameter $b \sim 0.21$ remains moderate with respect to 1, that is, the isotropic component. Regarding the boundary condition, the radius $R(\theta)$ corresponds to a perturbated disk of radius R_0. The second greatest term $|c_4| \sim 0.13$ is reasonably small compared to the first and others decrease quickly (see Figure 1A). Thus, in order to find an approximate solution to this problem, one can write the first order variation of the solution with respect to these parameters.

$$\underline{u} = \underline{u}_{00} + b\underline{u}_{10} + c\underline{u}_{01} \tag{13}$$

with $c = c_4$ the leading disk perturbation term. Inserting this expression in the (E) problem, three independent problems arise to find $\underline{u}_{00}$, $\underline{u}_{10}$ and $\underline{u}_{01}$:

$$\begin{array}{ll} (\Omega) & \left| \begin{array}{l} \underline{\underline{\epsilon}}^{\kappa}(r) = \left(\kappa_{\Sigma}^2 - \kappa_{\Delta}^2\right)\dfrac{r^2}{8}\begin{bmatrix} 1 & 0 \\ 0 & 0 \end{bmatrix} \\ \underline{\sigma}_{00} = \underline{\underline{\underline{\underline{C}}}}^{i} : \left(\dfrac{1}{2}\left({}^{t}\underline{\nabla}\underline{u}_{00} + \underline{\nabla}\underline{u}_{00}\right) + \underline{\underline{\epsilon}}^{\kappa}\right) \\ \underline{\nabla}.\left(\underline{\sigma}_{00}\right) = \underline{0} \end{array} \right. \\ (\partial\Omega) & \left| \underline{\sigma}_{00}.\underline{e}_r = \underline{0} \right. \end{array} \tag{E00}$$

This first problem corresponds to a curved isotropic disk.

$$\begin{array}{ll} (\Omega) & \left| \begin{array}{l} \underline{\underline{\epsilon}}^{\kappa}(r) = \left(\kappa_{\Sigma}^2 - \kappa_{\Delta}^2\right)\dfrac{r^2}{8}\begin{bmatrix} 1 & 0 \\ 0 & 0 \end{bmatrix} \\ \underline{\sigma}_{10} = \dfrac{1}{2}\underline{\underline{\underline{\underline{C}}}}^{i} : \left({}^{t}\underline{\nabla}\underline{u}_{10} + \underline{\nabla}\underline{u}_{10}\right) + \underline{\underline{\underline{\underline{C}}}}^{\mu} : \left(\dfrac{1}{2}\left({}^{t}\underline{\nabla}\underline{u}_{00} + \underline{\nabla}\underline{u}_{00}\right) + \underline{\underline{\epsilon}}^{\kappa}\right) \\ \underline{\nabla}.\left(\underline{\sigma}_{10}\right) = \underline{0} \end{array} \right. \\ (\partial\Omega) & \left| \underline{\sigma}_{10}.\underline{e}_r = \underline{0} \right. \end{array} \tag{E10}$$

This second problem corresponds to a curved anisotropic (cubic) disk.

$$\begin{array}{ll} (\Omega) & \left| \begin{array}{l} \underline{\sigma}_{01} = \dfrac{1}{2}\underline{\underline{\underline{\underline{C}}}}^{i} : \left({}^{t}\underline{\nabla}\underline{u}_{01} + \underline{\nabla}\underline{u}_{01}\right) \\ \underline{\nabla}.\left(\underline{\sigma}_{01}\right) = \underline{0} \end{array} \right. \\ (\partial\Omega) & \left| \underline{\sigma}_{01}.\underline{e}_r + \underline{\sigma}_{00}.\underline{e}_{\theta}\sum_{n=1}^{N} n\frac{c_n}{c_4}\sin(n\theta) + R_0\frac{\partial}{\partial r}\left(\underline{\sigma}_{00}\right).\underline{e}_r\sum_{n=1}^{N}\frac{c_n}{c_4}\cos(n\theta) = \underline{0} \right. \end{array} \tag{E01}$$

This third problem corresponds to an isotropic pseudo-square.

3 | STRESS DISTRIBUTIONS

Regarding the present application, the radius R_0 does not correspond to the cell half-side L (see Figure 1B). It is the radius of the 0^{th} order term of the pseudo-square Fourier series coefficients (see Appendix A.1.1). In the following the radius used is $R_0 = L/0.9$. The upcoming results are presented with a set of parameters that aims to represent a M0 cell. Therefore, $R_0 = 87\text{mm}(L = 78\text{mm})$ and $W = 0.2\text{mm}$. Regarding material properties, the parameters are $E = 130\text{GPa}, \nu =$

0.278 and $b = 0.21$.[20] The solution to problem (E_{00}) predicts a membrane stress:

$$\underline{\underline{\sigma}}(r) = \frac{E}{64}\left(\kappa_\Sigma^2 - \kappa_\Delta^2\right)\begin{bmatrix} R_0^2 - r^2 & 0 \\ 0 & R_0^2 - 3r^2 \end{bmatrix} \quad (14)$$

Stress tensors are always symmetric and thus diagonalizable. As a consequence, they can be summarized using their eigenvalues ranked from the highest to the smallest. The first one, that is, the first principal stress σ_I, is the relevant metric to predict the failure of brittle materials such as silicon. Since the present stress tensor is already diagonal, the principal stresses are in the radial and ortho-radial directions, respectively. σ_I distribution is presented in Figure 2A with $\kappa = \kappa_\Sigma$ and $\kappa_\Delta = 0$. In this case, σ_I is oriented along the radial direction. In the figure, the area of high stress is located near the disk center. With the present set of parameters, the highest stress is 61.5 MPa. σ_I map is presented on Figure 2B with $\kappa_\Sigma = 0$. In this second case, σ_I is oriented along the orthoradial direction and the highest stress value is twice the previous one (123 MPa). It is located in the vicinity of the outer boundary.

Using the flexure strain tensor (8), the highest stress σ_{max} can be computed for a given curvature. Using Equation (14), the ratio of membrane to flexure stress can be computed at the same position. The corresponding result is called the von Kármán number, and it writes $R_0^2\kappa/(16W)$.[14] Please note that this ratio is uniquely defined by the system size, thickness, and the applied curvature. σ_{max} is presented on Figure 2C as a function of $1/\kappa$. As the curvature radius decreases, the maximum stress switches from flexure to membrane dominated with isotropic and saddle shape conformations. The transition presented in Figure 2C corresponds to a von Kármán number equal to 1. For a cell characteristic fracture stress of $\sigma_c = 120$ MPa, the transition is expected prior to failure. Furthermore, the curvature radius at failure is about one order of magnitude smaller because of this contribution.

Using the analytical expressions, both the membrane and the flexure stress distributions can be computed for every couple of values $\kappa_\Sigma, \kappa_\Delta$. This couple of values describes the entire space of constant curvatures. Therefore, for each configuration the maximum curvature prior to failure can be computed for a given value of σ_c. This prediction is presented on Figure 2D. In the figure, the solid line represents

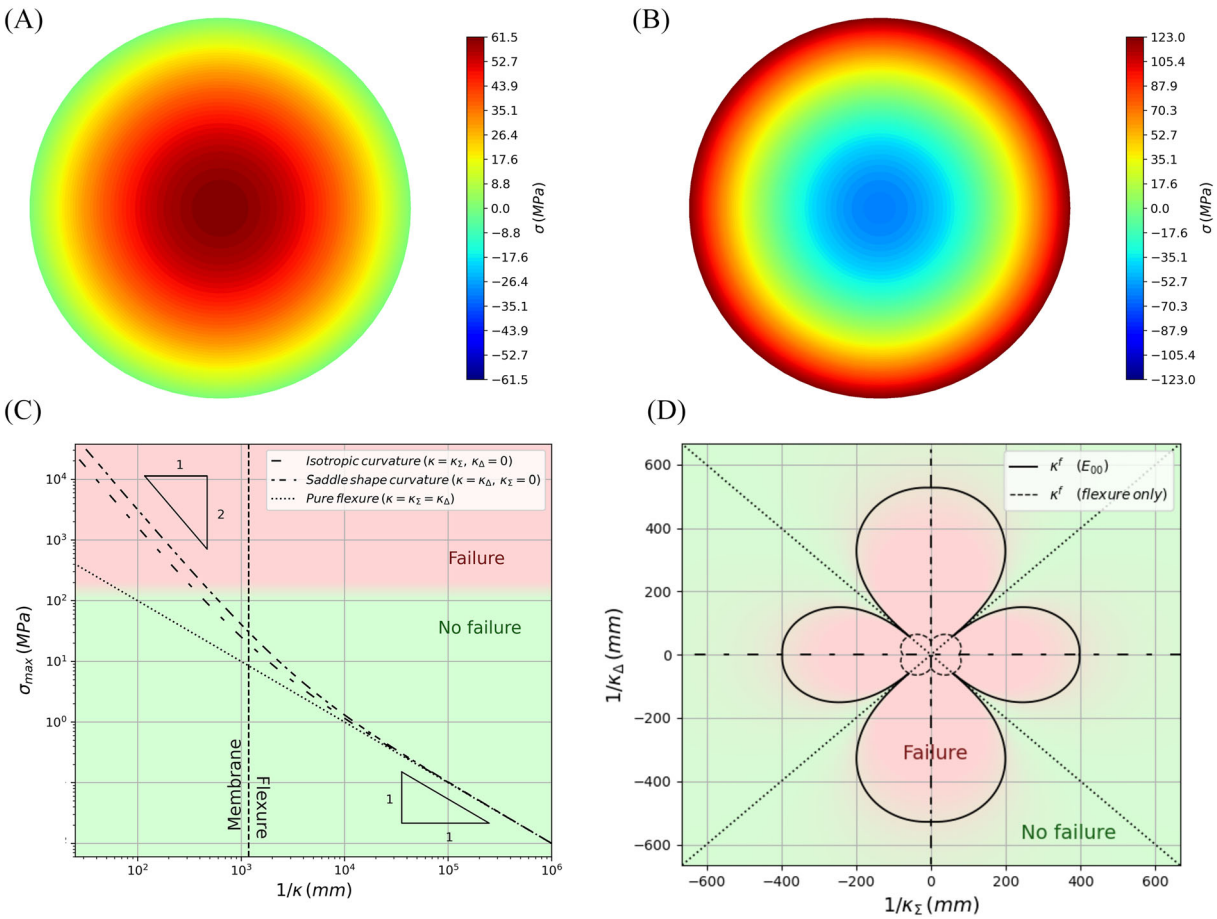

FIGURE 2 (E_{00}) membrane stresses (A) $\sigma_I(\kappa = \kappa_\Sigma, \kappa_\Delta = 0)$ and (B) $\sigma_I(\kappa = \kappa_\Delta, \kappa_\Sigma = 0)$. (C) Maximal total stress as a function of κ. (D) Failure boundary in curvature space. Parameters used are: $L = 78\text{mm}(R_0 = 87\text{mm})$ and $\kappa = 2 \times 10^{-3}\text{mm}^{-1}, E = 130\text{GPa}, \nu = 0.278$ and $\sigma_c = 120\text{MPa}$ [Colour figure can be viewed at wileyonlinelibrary.com]

the failure limit as predicted by problem (E_{00}) solution. The inner dashed limit corresponds to the failure limit in pure flexure (without any membrane contribution). Both limits are equivalent along the diagonals (pure flexure) or their vicinities. However, this situation appears to be an unrepresentative exception. In practice, it means that the risks of failure uncountered with modules in pure flexure (curved in a single direction) are very different from the ones encountered in other cases. The first case causes less intense stresses than the second one. Please note that the curvature may be because of the module normal shape or the consequence of a mechanical loading.

Problem (E_{10}) takes into account the anisotropic behavior of mono-crystalline silicon. Its solution is presented in Appendix A.1.4. This solution contributes in proportion to the anisotropic factor $(b = 0.21)$. The principal membrane stress σ_I and the shear membrane stress are presented in Figure 3A–C. The contribution of the anisotropic term is twofold. First, it breaks the stress invariance in rotation. Second, it increases the inner and outer maximum tensile stress by 18% (FEM computations predict an increase of 13%). One can notice that the shear stress is not nil at the outer boundary despite the definition of problem (E_{10}). This is due to the first order approximation, shear stresses are therefore proportional to b^2. Their intensities gives an idea about the relevance of the first order model. The error provides another mean to assess this model accuracy to ~10%. Using the anisotropic solution, the curvature at failures is computed and presented in Figure 3D. In the figure, the curvature at failure is weakly impacted by the anisotropic nature of mono-crystalline silicon.

Problem (E_{01}) describes the membrane mechanical equilibrium for a disk turned into a pseudo-square. A way to compute its solution for every perturbation frequency is presented in Appendix A.1.5. The membrane stress tensor first principal stress σ_I is presented in Figure 4A,B. The corresponding shear stress is presented in Figure 4C. Regarding problem (E_{01}), the bulk equation has no second member. Therefore, the additional terms must rely on the homogenous solutions (see Appendix A.1.2). These solutions take the form $r^{n\pm1}\cos(n\theta+\phi)$ in displacement. Please note that the first perturbation term which is not nil has a frequency $n = 4$. Thus, the lower order homogenous term scales in proportion to r^3 in displacement and to r^2 in strain. As a consequence, the shape impact near the system center is negligible. However, 10% higher levels of radial stresses are predicted along each corner direction. According to FEM simulations, the membrane stress levels are 7% lower near the system center and radial stresses are constant in the central area. This result indicates that the first order model is only of moderate accuracy. Regarding σ_I in the saddle shape case, the maximum stress is, once again, located in

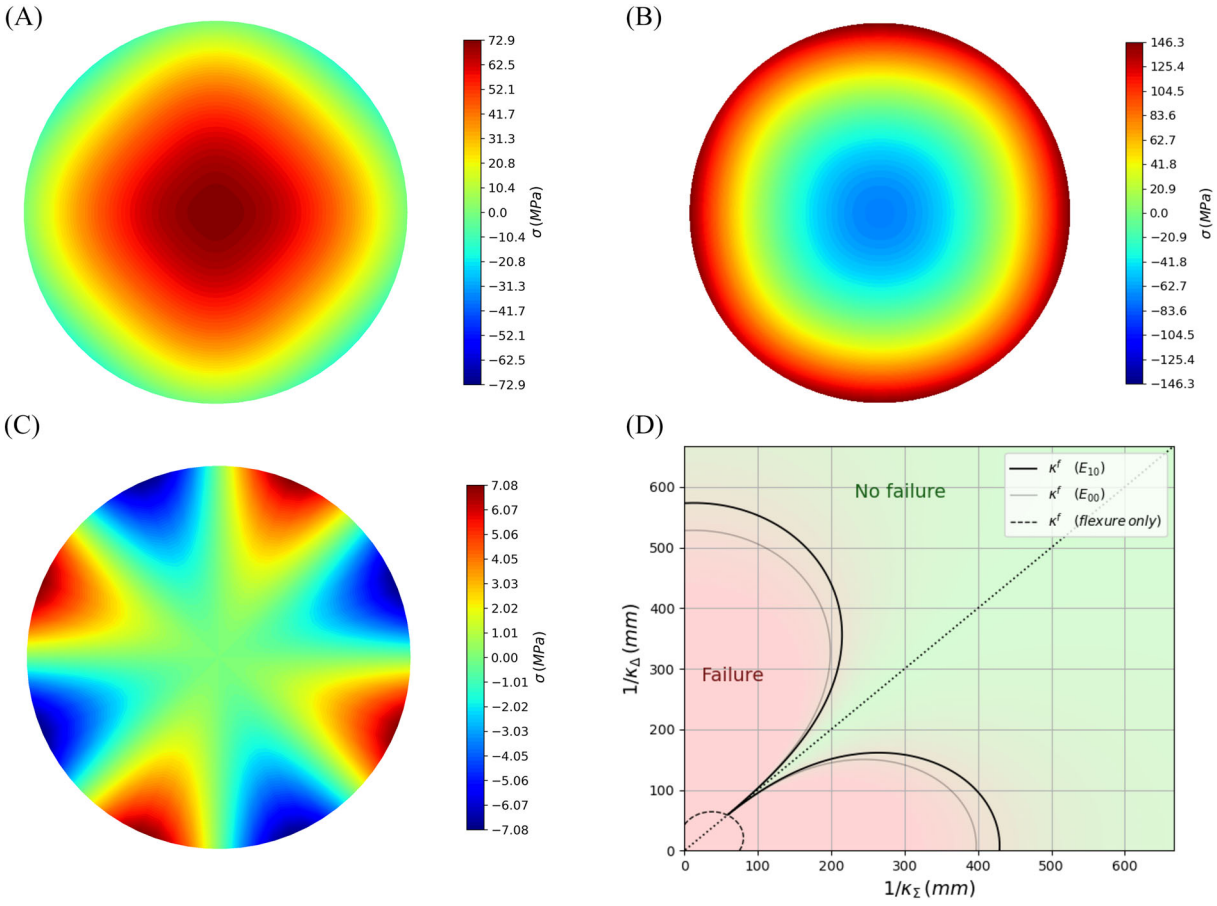

FIGURE 3 (E_{00}) membrane stresses (A) σ_I $(\kappa = \kappa_\Sigma, \kappa_\Delta = 0)$, (B) σ_I $(\kappa = \kappa_\Delta, \kappa_\Sigma = 0)$, and (C) $\sigma_{r\theta}$ $(\kappa = \kappa_\Sigma, \kappa_\Delta = 0)$. (D) Failure boundary in curvature space. Parameters used are as follows: $L = 78$ mm ($R_0 = 87$ mm) and $\kappa = 2 \times 10^{-3}$ mm^{-1}, $E = 130$ GPa, $b = 0.21$, $\nu = 0.278$, and $\sigma_c = 120$ MPa [Colour figure can be viewed at wileyonlinelibrary.com]

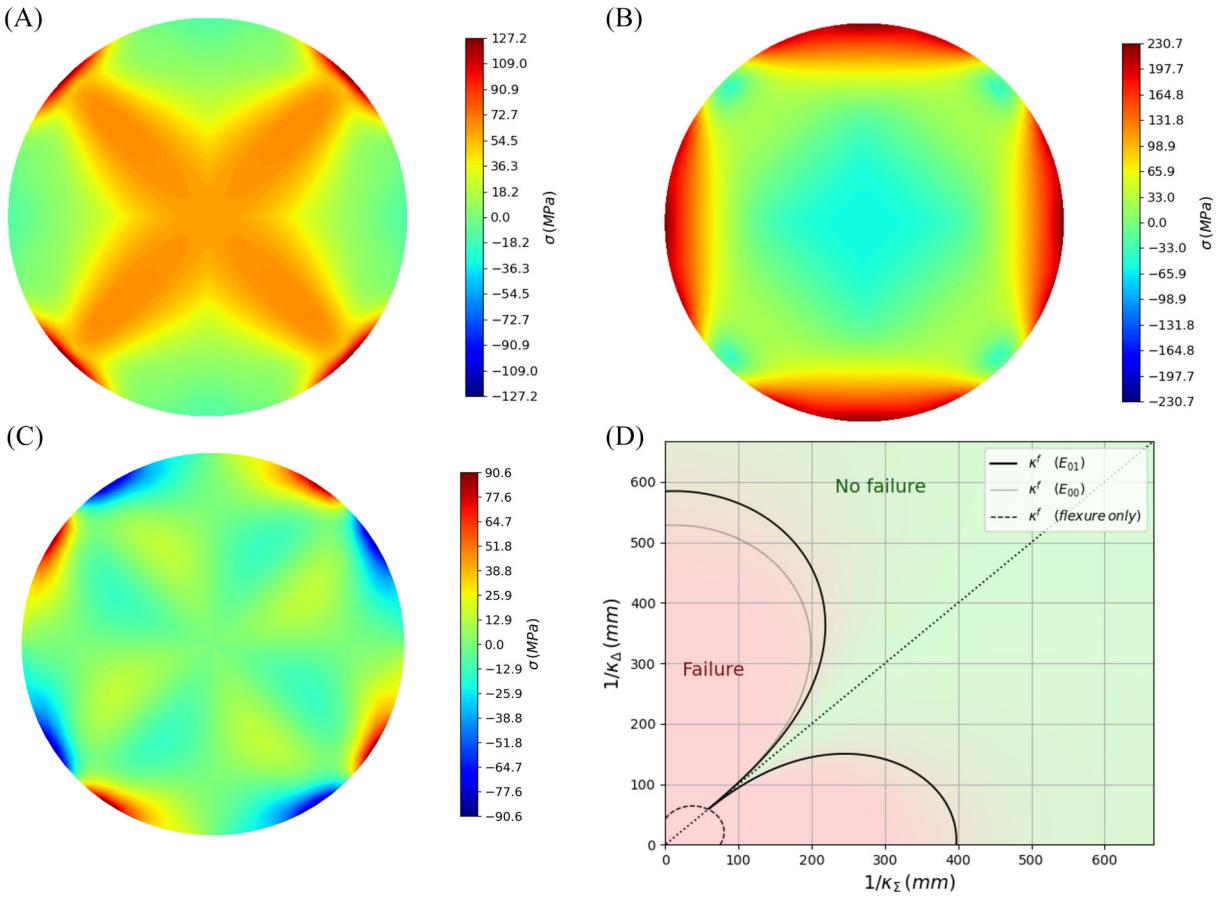

FIGURE 4 (E_{01}) membrane stresses (A) σ_I ($\kappa = \kappa_\Sigma$, $\kappa_\Delta = 0$), (B) σ_I ($\kappa = \kappa_\Delta$, $\kappa_\Sigma = 0$), and (C) $\sigma_{r\theta}$ ($\kappa = \kappa_\Sigma$, $\kappa_\Delta = 0$). (D) Failure boundary in curvature space. Parameters used are as follows: $L = 78$ mm ($R_0 = 87$ mm), $c = 0.13$, $\kappa = 2 \times 10^{-3}$ mm^{-1}, $E = 130$ GPa, $\nu = 0.278$, and $\sigma_c = 120$ MPa [Colour figure can be viewed at wileyonlinelibrary.com]

the vicinity of the outer boundary. At the pseudo-square boundary ($r = L = 78$ mm, $\theta = 0$), inside the mapped disk of radius $R_0 = 87$ mm presented in Figure 4B, the predicted maximum stress is 24% higher than the isotropic disk one. With FEM computations the prediction at the same location is very close (26%). Finally, intense shear stresses are predicted near the pseudo-square corners (see Figure 4C). The corresponding values confirm that the accuracy of the first order model is limited. Using the maximum tensile stress at the system center and outer boundary for the isotropic and saddle shape curvature respectively, the failure limit is computed and presented on Figure 4D. In this case, the failure radius is not strongly impacted either.

4 | RELEVANCE AND PRACTICAL CONSEQUENCES

In the last section, the computations were performed with the parameters of a typical M0 PV cell. With these dimensions, the radius of curvature at failure is $\kappa \sim 1$ m^{-1}. The product of cell size and curvature is $\kappa L \sim 8 \times 10^{-2}$. Thus, the small curvature hypothesis made in Section 2.1 is reasonable. At this curvature, the corresponding maximum displacement is $(\kappa L^2)/2 \sim 3$ mm. In a standard module, the encapsulant thickness is ~1 mm. As a consequence, the cell does not have a sufficient space to adapt its conformation and relax itself. Furthermore, the total energy stored in the cell due to membrane stresses scales as $E^{el} \sim EWL^2(L\kappa/64)^2$. Since the stored energy scales as the product of the displacement times the effort $(\kappa L^2/2)(L^2 P)$, the pressure required to curve the cell is $P \sim 2EW\kappa/64^2$. In the present problem, it gives $P \sim 0.03$ MPa. The encapsulant shear modulus is typically in the range 1–100 MPa,[21] but its bulk modulus is substantially greater (~1 GPa[22]). Therefore, this level of stress is not sufficient to cause substantial strains within the encapsulant. Therefore, the hypothesis of an imposed conformation is realistic.

In practical applications, residual stresses exist within cells at ambiant temperature due to the interconnection or lamination process. In both cases, the materials in contact with the cells, that is, the ribbons and the encapsulant, apply a mechanical loading on them. As a consequence, one should question the hypothesis of no external loading performed to write Equations (10) and (13). However, since the system (13) is linear, the superposition principle is valid. As a consequence, the solution with an external loading and a curvature would be the sum of the solution with an external loading (and no curvature) and the solution with a curvature (and no external loading). The

present work is restricted to the second contribution. The first one (residual stresses) goes beyond the scope of the present paper. Numerous works regarding this issue can be found in the literature.[23–26]

Membrane stresses scale in proportion to $(L\kappa)^2$. As a consequence, decreasing cell sizes is an efficient way to reduce this contribution. In contrast, the thickness W impacts the flexure stress which scales in proportion to $W\kappa$. Therefore, to reduce stresses within a given curved module, one should try first to compute the Kármán number. If this number is greater than 1 then cell size L is the key parameter. Otherwise, the cell thickness W is. In the later case, other contributions may be affected by cell thickness (for instance residual stresses[24]). Please note that the parameters used in the present work: $L = 78$ mm and $W = 0.2$ mm provide a low membrane to flexure ratio since it scales in proportion to $L^2\kappa/W$ and cells sizes are and tend to be larger and thinner.[27,28]

Another current trend is to use fractions of cells.[28] In the case of a strip of length $2L_x$ and width $2L_y$ such as represented on Figure 5A, the in-plane equilibrium can be solved in an asymptotic case, that is, an extremely thin strip ($L_x \gg L_y$). A complete derivation is presented in Section A.1.6. This model still corresponds to the description provided in Section 2.1. As a consequence, its solution is independent of the curvature orientation and the isotropic and saddle shape solutions are the opposite of one another. The evolution of the maximum tensile stress has been computed with this analytical model and FEM simulations. The results are presented in Figure 5B. Surprisingly, the asymptotic model is already in good agreement with FEM predictions for a ratio as low as $L_y/L_x = 1/2$. The model solution predicts that membrane stresses scale in proportion to $(L_y\kappa)^2$. The curvature at failure for aspect ratio of 1 (pseudo-square), 1/2, 1/3, 1/4, and 1/6 are reported in Figure 5C. Note the strong decrease of the failure area is due to the increased aspect ratio. In contrast, the impact of cell format is presented in Figure 5D with an aspect ratio of 1. Each cell format corresponds to an in-plane size. Namely, M0, M6, M10, and M12 correspond to sizes of $2L = 156$, 166, 200, and 210 mm, respectively. In the figure, larger cell sizes have substantially larger curvature radius at failure. Finally, the influence of cell thickness is presented on Figure 5E. At failure, the influence of this parameter is quite limited.

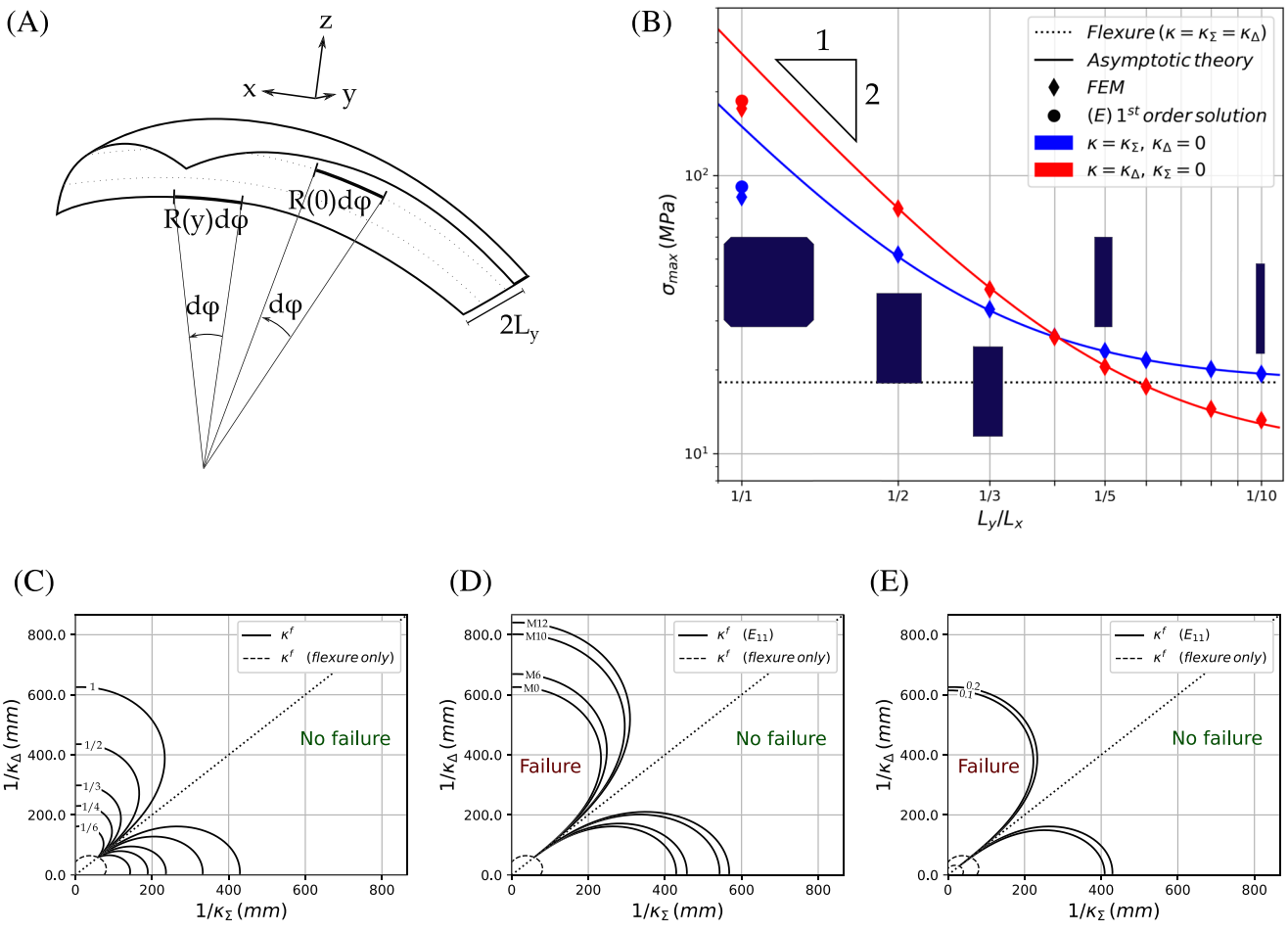

FIGURE 5 (A) Sketch of a curved strip. (B) Evolution of maximum tensile stress as a function of the aspect ratio L_y/L_x. In this figure, colors represent the same conformation for all types of computations (FEM, asymptotic and (*E*) 1st order solution). Curvature limit for (C) aspect ratios from 1 to 1/6 with $L_x = 78$ mm (D) cell standard size from *M*0 to *M*12, and (E) cell thickness from 0.1 to 0.2 mm. When not specified, the aspect ratio is 1, $L = 78$ mm (M0) and $W = 0.2$ [Colour figure can be viewed at wileyonlinelibrary.com]

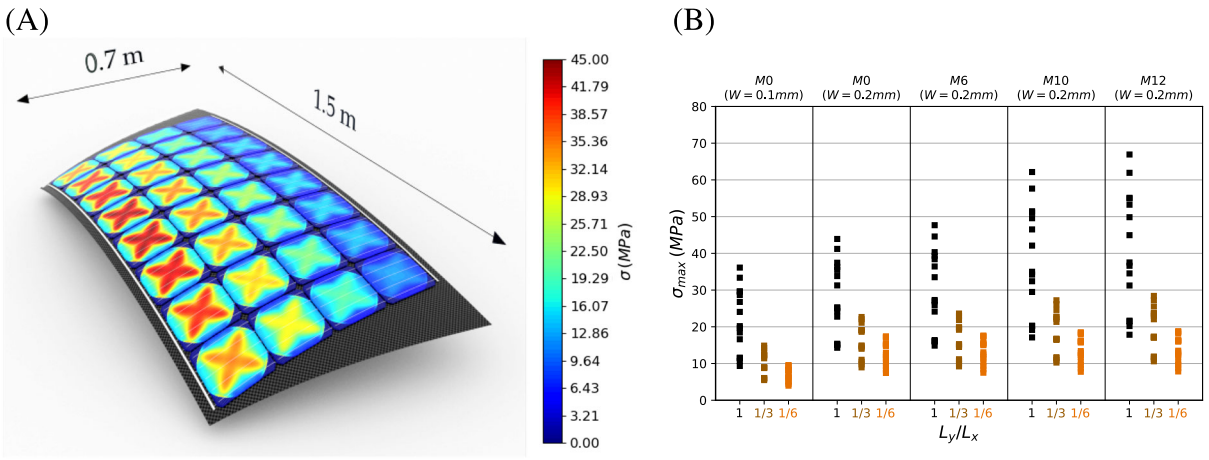

FIGURE 6 (A) Curved module with pseudo-square M0 cells of thickness $W = 0.2$ mm. Cells texture represent the local σ_I stress computed with the present model. (B) Evolution of the maximum stress σ_I for all cells in the curved module using different standard cell size and aspect ratios [Colour figure can be viewed at wileyonlinelibrary.com]

In order to highlight the relevance of this solution in a practical situation, a case study is presented: The integration of cells in an imaginative curved structure, that is, the car hood represented in Figure 6A. In the present example, curvature radii are about of a few meters and they vary slowly at the module scale. Both of these characteristics are typical of vehicle-integrated photovoltaics (VIPV). The equation describing this shape is presented in Appendix A.1.7. In the figure, the first principal stress within cells predicted by the present model are represented with colors. The highest stresses are at about 45 MPa with thick ($W = 0.2$ mm) M0 ($L = 78$mm) cells. The stress distribution in cells is membrane dominated. The maximum stress in each cell is presented in Figure 6B for different cell sizes and aspect ratios. In order to make the comparison meaningful, local curvatures are identical with each cell format, thickness or fraction. In the figure, maximum stresses increase substantially with cell size. For a pseudo-square shape ($L_y/L_x = 1$), the highest stress increases up to 65 MPa with M12 cells. However, stresses decrease quickly when fractions of cells are used instead of full ones. For instance, the use of thirds of cells decreases the maximum stress from 45 to 25 MPa with M0 format and from 65 to 30MPa with M12 one. In contrast, reducing cell thickness has a limited impact. With the M0 format decreasing cell thickness from 0.2 to 0.1 mm decreases the maximum stress from 45 to 35MPa.

Therefore, the use of fractions of cell is a promising solution to make modules of important curvatures or to reduce stresses within less curved one. Note, that the process used to produce fractions of cell may induce new defaults and thus reduce the characteristic fracture stress.[2–5] Another current trend is to use alternative architectures based on fractions of cells, that is, shingles.[27] However, in PV shingles, the cells are rigidly bonded to one another. As a consequence, the characteristic length is not expected to be the side of a fraction of cell but rather the side of the assembly. Therefore, the membrane contribution is expected to be high.

Finally, in order to design a module for PV applications, a certain margin must be taken to ensure the integrity of cells and prevent additional undesired effects. In this scenario, the target module curvature may be quite different from the limits or cases reported in the present work or a more specific failure criterion may be applied to the stress field in order to predict failure. In such situations, solutions to problems (E_{00}), (E_{10}), (E_{01}) and the asymptotic one are still expected to be of relevance. They are also believed to be of interest in similar problems which imply to curve silicon wafers.[18,19] To make their use simpler, an open python code is provided in the attached material. This code purpose is to display the solutions as functions of the input parameters.

5 | CONCLUSION

The production of conventional but curved modules causes the cells to curve inside them. Such a constraint induces both flexure and membrane stresses. With standard cells dimensions and for curvatures in the range 1–5 m, membrane stresses dominates flexure ones. In contrast with flexure stresses, membrane stresses are not uniformly distributed within cells. They are strongly sensitive to cells sizes and aspect ratios. As a consequence for a designer, the main degree of freedom to reduce stresses with a cell is to reduce cell sizes or to increase the aspect ratio. The second is probably more suitable since fractions of cells are already widely spread and their use will continue to grow. For specific applications, the curvature may be close to pure flexion. Even in such situations, small Gaussian curvature can cause important membrane stresses. As a consequence, cell sizes and aspect ratio may still be the problem key parameters. Therefore, cells thickness is a second order one. Its relevance is mainly limited to pure flexure cases. Furthermore, other contributions (for instance, residual thermomechanical stresses) should also be accounted for to design a curved module. Finally, the solutions presented in this work are believed to be of importance to predict and therefore reduce internal stresses within mono-crystalline silicon cells.

ACKNOWLEDGMENTS

This work has been supported by the *Commissariat à l'Énergie Atomique et aux Énergies Alternatives* (CEA), the *Institut pour la Transition Energétique* (INES.2S), and the MicroFlex project of the Carnot Energies du Futur.

DATA AVAILABILITY STATEMENT

The data that support the findings of this study are available from the corresponding author upon reasonable request.

REFERENCES

1. Hopcroft MA, Nix WD, Kenny TW. What is the Young's modulus of silicon? *J Microelectromech Syst*. 2010;19(2):229-238.
2. Coletti G, Van Der Borg NJCM, De Iuliis S, Tool CJJ, Geerligs LJ. Mechanical strength of silicon wafers depending on wafer thickness and surface treatment. In: Proc. of the 21st European Photovoltaic Solar Energy Conf. Dresden, Germany; 2006.
3. Möller HJ, Funke C, Rinio M, Scholz S. Multicrystalline silicon for solar cells. *Thin Solid Films*. 2005;487(1-2):179-187.
4. Sekhar H, Fukuda T, Tanahashi K, et al. Mechanical strength problem of thin silicon wafers (120 and 140 μm) cut with thinner diamond wires (Si kerf 120→ 100 μm) for photovoltaic use. *Materials Sci Semiconduct Process*. 2020;119:105209.
5. Wang L, Gao Y, Pu T, Yin Y. Fracture strength of photovoltaic silicon wafers cut by diamond wire saw based on half-penny crack system. *Eng Fract Mech*. 2021;251:107717.
6. McLaughlin JC, Willoughby AFW. Fracture of silicon wafers. *J Crystal Growth*. 1987;85(1-2):83-90.
7. Sekhar H, Fukuda T, Kida Y, Tanahashi K, Takato H. The impact of damage etching on fracture strength of diamond wire sawn monocrystalline silicon wafers for photovoltaics use. *Japanese J Appl Phys*. 2018;57(12):126501.
8. Pérez R, Gumbsch P. Directional anisotropy in the cleavage fracture of silicon. *Phys Rev Lett*. 2000;84(23):5347.
9. Carton L, Riva R, Nelias D, Fourmeau M, Coustier F, Chabli A. Comparative analysis of mechanical strength of diamond-sawn silicon wafers depending on saw mark orientation, crystalline nature and thickness. *Solar Energy Mater Solar Cells*. 2019;201:110068.
10. Barredo J, Parra V, Guerrero I, Fraile A, Hermanns L. On the mechanical strength of monocrystalline, multicrystalline and quasi-monocrystalline silicon wafers: a four-line bending test study. *Progress Photovoltaics: Res Appl*. 2014;22(12):1204-1212.
11. Borrero-López O, Vodenitcharova T, Hoffman M, Leo AJ. Fracture strength of polycrystalline silicon wafers for the photovoltaic industry. *J Am Ceramic Soc*. 2009;92(11):2713-2717.
12. Funke C, Kullig E, Kuna M, Möller HJ. Biaxial fracture test of silicon wafers. *Adv Eng Mater*. 2004;6(7):594-598.
13. Landau LD, Lifshitz EM. Theory of elasticity (Pergamon Press, Oxford, 1959); 1970.
14. Paulsen JD. Wrapping liquids, solids, and gases in thin sheets. arXiv preprint arXiv:180407425; 2018.
15. Aly SP, Ahzi S, Barth N, Abdallah A. Numerical analysis of the reliability of photovoltaic modules based on the fatigue life of the copper interconnects. *Solar Energy*. 2020;212:152-168.
16. Hasan O, Arif AFM. Performance and life prediction model for photovoltaic modules: effect of encapsulant constitutive behavior. *Solar Energy Mater Solar Cells*. 2014;122:75-87.
17. Song WJR, Tippabhotla SK, Tay AAO, Budiman AS. Effect of interconnect geometry on the evolution of stresses in a solar photovoltaic laminate during and after lamination. *Solar Energy Materials Solar Cells*. 2018;187:241-248.
18. Chambion B, Nikitushkina L, Gaeremynck Y, et al. Tunable curvature of large visible CMOS image sensors: towards new optical functions and system miniaturization. In: 2016 IEEE 66th Electronic Components and Technology Conference (ECTC) IEEE; 2016:178-187.
19. Tekaya K, Fendler M, Inal K, Massoni E, Ribot H. Mechanical behavior of flexible silicon devices curved in spherical configurations. In: 2013 14th International Conference on Thermal, Mechanical and Multi-Physics Simulation and Experiments in Microelectronics and Microsystems (EUROSIME) IEEE; 2013:1-7.
20. Hall JJ. Electronic effects in the elastic constants of n-type silicon. *Phys Rev*. 1967;161(3):756.
21. Eitner U, Kajari-Schröder S, Köntges M, Brendel R. Non-linear mechanical properties of ethylene-vinyl acetate (EVA) and its relevance to thermomechanics of photovoltaic modules. In: 25th European Photovoltaic Solar Energy Conference; 2010; Valencia, Spain:1-3.
22. Burns J, Dubbelday PS, Ting RY. Dynamic bulk modulus of various elastomers. *J Polymer Sci Part B: Polymer Phys*. 1990;28(7):1187-1205.
23. Beinert AJ, Romer P, Büchler A, Haueisen V, Aktaa J, Eitner U. Thermomechanical stress analysis of PV module production processes by raman spectroscopy and FEM simulation. *Energy Proc*. 2017;124:464-469.
24. Beinert AJ, Romer P, Heinrich M, Aktaa J, Neuhaus H. Thermomechanical design rules for photovoltaic modules. *Progress Photovoltaics: Res Appl*. 2022:1-13.
25. Rendler LC, Romer P, Beinert AJ, et al. Thermomechanical stress in solar cells: contact pad modeling and reliability analysis. *Solar Energy Materials Solar Cells*. 2019;196:167-177.
26. Tippabhotla SK, Song WJR, Tay AAO, Budiman AS. Effect of encapsulants on the thermomechanical residual stress in the back-contact silicon solar cells of photovoltaic modules—a constrained local curvature model. *Solar Energy*. 2019;182:134-147.
27. International technology roadmap for photovoltaic (ITRPV); 2021.
28. Wilson GM, Al-Jassim M, Metzger WK, et al. The 2020 photovoltaic technologies roadmap. *J Phys D: Appl Phys*. 2020;53(49):493001.

How to cite this article: Charpentier J-B, Duigou T, Chambion B, Voarino P, Chabuel F. Photovoltaic integration in curved parts: Mechanical limits and key parameters from a theoretical point of view. *Prog Photovolt Res Appl*. 2023;1-14. doi:10.1002/pip.3666

APPENDIX A

A.1 | Simplification of $\underline{\underline{\epsilon}}^k$

The expression of $\underline{\underline{\epsilon}}^k$ is the sum of three terms of different frequencies:

$$\underline{\underline{\epsilon}}^k(r,\theta) = \frac{r^2}{8}\left(\begin{bmatrix}\kappa_\Sigma^2+\frac{\kappa_\Delta^2}{2} & 0\\ 0 & \frac{\kappa_\Delta^2}{2}\end{bmatrix} + \kappa_\Delta\kappa_\Sigma[2\cos(2\theta)-\sin(2\theta)-\sin(2\theta)0] + \frac{\kappa_\Delta^2}{2}[\cos(4\theta)-\sin(4\theta)-\sin(4\theta)-\cos(4\theta)]\right) \tag{A15}$$

If ones defines a displacement field $\underline{u}_n$ such that

$$\underline{u}_n(r,\theta) = r^3[A_n\cos(n\theta)B_n\sin(n\theta)] \tag{A16}$$

Then, according to Equation (3), the corresponding in-plane strain writes

$$\underline{\underline{\epsilon}}_n^p(r,\theta) = r^2\begin{bmatrix} 3A_n\cos(n\theta) & \frac{1}{2}(2B_n-nA_n)\sin(n\theta)\\ \frac{1}{2}(2B_n-nA_n)\sin(n\theta) & (nB_n+A_n)\cos(n\theta)\end{bmatrix} \tag{A17}$$

Using this expression along with Equation (4), the three independent components of the term with $n=2$ are canceled with $A_2=-2\kappa_\Delta\kappa_\Sigma/3$ and $B_2=\kappa_\Delta\kappa_\Sigma/3$. The three independent components of the term with $n=4$ are canceled with $A_4=-\kappa_\Delta^2/6$ and $B_4=\kappa_\Delta^2/6$. Therefore, the corresponding terms of $\underline{\underline{\epsilon}}^k$ will not appear in $\underline{\underline{\epsilon}}$ and thus induce elastic strain in the system. Regarding the term with $n=0$, no value of A_0 can cancel the three independent components of $\underline{\underline{\epsilon}}^k$ for every values of κ_Δ and κ_Σ. However, there is a solution $A_0=-\kappa^2/2$ if $\kappa_\Sigma^2=\kappa_\Delta^2=\kappa$. This implies that the following $\underline{\underline{\epsilon}}^\kappa$ is equivalent to the previous one:

$$\underline{\underline{\epsilon}}^\kappa(r) = \frac{r^2}{8}\left(\begin{bmatrix}\kappa_\Sigma^2+\frac{\kappa_\Delta^2}{2} & 0\\ 0 & \frac{\kappa_\Delta^2}{2}\end{bmatrix} - \begin{bmatrix}3\frac{\kappa^2}{2} & 0\\ 0 & \frac{\kappa^2}{2}\end{bmatrix}\right) \tag{A18}$$

for every value of κ. As a consequence, the curvature strain for $\kappa_\Sigma^2=\kappa^2,\kappa_\Delta^2=0$ is exactly opposite to the curvature strain for $\kappa_\Sigma^2=0,\kappa_\Delta^2=\kappa^2$. Finally, for a linear problem without external loading, the solution to one of the two gives the solution to the second problem. Therefore, solving one problem provides the solution for every set of curvatures (since it can always be decomposed into the two specific cases discussed before). In the text, the reference problem will be treated with Equation (A18) in the case $\kappa^2=\kappa_\Delta^2$. The corresponding curvature strain tensor writes

$$\underline{\underline{\epsilon}}^\kappa(r) = \frac{r^2}{8}\begin{bmatrix}\kappa_\Sigma^2-\kappa_\Delta^2 & 0\\ 0 & 0\end{bmatrix} \tag{A19}$$

These are results are deeply connected to the Gaussian curvature and the *theorema egregium*. In our problem, the Gaussian curvature writes $\kappa_1\kappa_2=4(\kappa_\Sigma^2-\kappa_\Delta^2)$. This quantity scales in proportion to membrane stresses.

A.1.1 | Fourier series of a pseudo-square

The pseudo-square shape is basically a square with a portion of circle at each of its corner. In the following, the square part corresponds to an angle θ_0. $R(\theta)$ writes

$$R(\theta) = \frac{1}{\cos(\theta)}\ \theta\in[0,\theta_0] \tag{A20}$$

$$R(\theta) = \frac{1}{\cos(\theta_0)}\ \theta\in\left[\theta_0,\frac{\pi}{4}\right] \tag{A21}$$

with a pseudo-square side of length 2. Thanks to the symmetry of the pseudo-square, this description is sufficient to represent it fully (only terms with a frequency divisible by 4 are not nil). Since R is a periodic function, its Fourier decomposition exists and is simpler to use in the present problem. In order to find its coefficient, the function $1/\cos(\theta)$ is approximated using a Taylor expansion:

$$\frac{1}{\cos(\theta)} \approx 1+\frac{1}{2}\theta^2+\frac{5}{24}\theta^4+\frac{61}{720}\theta^6 \tag{A22}$$

Then, Fourier series coefficients are computed with this approximation:

$$d_0 = \frac{4}{\pi}\int_0^{\frac{\pi}{4}-\theta_0}\left(1+\frac{1}{2}\theta^2+\frac{5}{24}\theta^4+\frac{61}{720}\theta^6\right)d\theta + \frac{2}{\pi}\int_{\frac{\pi}{4}-\theta_0}^{\frac{\pi}{4}}\frac{1}{\cos(\theta_0)}d\theta \tag{A23}$$

$$d_n = \frac{8}{\pi}\int_0^{\frac{\pi}{4}-\theta_0}\left(1+\frac{1}{2}\theta^2+\frac{5}{24}\theta^4+\frac{61}{720}\theta^6\right)\cos(n\theta)d\theta + \frac{4}{\pi}\int_{\frac{\pi}{4}-\theta_0}^{\frac{\pi}{4}}\frac{\cos(n\theta)}{\cos(\theta_0)}d\theta \tag{A24}$$

with $n>0$ and n divisible by 4 (other coefficients are nil). Finally, these functions are computed with I_{mn} and J_n:

$$I_{mn} = \int_0^{\theta_0}\theta^m\cos(n\theta)d\theta \tag{A25}$$

$$J_n = \int_{\theta_0}^{\frac{\pi}{4}}\cos(n\theta)d\theta \tag{A26}$$

which are can be computed using the following relations:

$$I_{m0} = \frac{\theta_0^{m+1}}{m+1} \tag{A27}$$

$$I_{0n} = \frac{\sin(n\theta_0)}{n} \tag{A28}$$

$$I_{mn} = \left(\frac{\theta_0^{m-1}}{n}\right)\left(\theta_0 \sin(n\theta_0) + \frac{m}{n}\cos(n\theta_0)\right) - \frac{m(m-1)}{n^2} I_{m-2n} \tag{A29}$$

$$J_0 = \frac{n\pi}{4} - \theta_0 \tag{A30}$$

$$J_n = \frac{1}{n}\left(\sin\left(\frac{n\pi}{4}\right) - \sin(n\theta_0)\right) \tag{A31}$$

with $m,n > 0$. Please note that the coefficients d_n describe a pseudo-square of half side 1 and a perturbated disk of radius d_0. In the manuscript, the perturbated disk described by the c_n coefficients has a radius equal to 1. Thus, $c_n = d_n/d_0$ and the pseudo-square half side L is different. It writes

$$\frac{L}{R_0} = \sum_n^N c_n \tag{A32}$$

In practice, $L \approx 0.9R_0$ for a typical (M_2 format) pseudo-square shape.

A.1.2 | Homogeneous solutions

Problems (E_{00}), (E_{10}) and (E_{01}) are based on the same partial differential equations but with different second members or boundary conditions. Thus, their homogeneous solutions take the same form. They must verify

$$\frac{1}{2}\underline{\nabla}.\left(\underline{\underline{\underline{C}}}^i : \left({}^t\underline{\underline{\nabla u}} + \underline{\underline{\nabla u}}\right)\right) = \underline{0} \tag{A33}$$

Considering a displacement field $\underline{u}$ of the form:

$$\underline{u}(r,\theta) = r^m[a_{rc}\cos(n\theta) + a_{rs}\sin(n\theta) a_{\theta c}\cos(n\theta) + a_{\theta s}\sin(n\theta)] \tag{A34}$$

and using their complex representation, one finds that Equation (A33) gives

$$\begin{bmatrix} n^2\nu - n^2 + 2m^2 - 2 & in(m\nu + m + \nu - 3) \\ in(m\nu + m - \nu + 3) & -2n^2 - m^2\nu + m^2 + \nu - 1 \end{bmatrix}.\underline{\hat{u}} = \underline{0} \tag{A35}$$

with $\underline{\hat{u}}$ the complex displacement field. This matrix is singular if its determinant is equal to zero. This condition writes

$$(m-(n+1))(m+(n+1))(m-(n-1))(m+(n-1)) = 0 \tag{A36}$$

The four solutions are $m = n \pm 1$ and $m = -(n \pm 1)$. In the present problem, the displacement field must be nil in $r = 0$. Therefore, the remaining solutions are $m = 1$ if $n = 0$ and $m = n \pm 1$ if $n > 0$. Please note that in the present problem, the numbers n must be integers since no displacement discontinuities are expected in the system. Therefore, the different m are themselves integers. Looking back at the three problems, one can notice that the components of $\underline{\underline{\epsilon}}^{\kappa}$ take the form described in Equation (A34). Furthermore, different operators in these problems will also produce terms of the same form. As a consequence the solutions must write as a series of such form.

A.1.3 | Solution to problem (E_{00})

As mentioned in Section A.1, solving a problem for a given set of curvatures κ_Σ, κ_Δ is equivalent to solving them all. Therefore in the upcoming sections we will assume: $\kappa_\Delta = 0$. As seen in Section A.1.2, the solutions to each one of the three problems must take similar forms like the one presented in Equation (A34). Prior to presenting their respective solutions, a notation is introduced: The coefficients of a displacement vector are named u_{00}^{rcmn} where r (or θ) is the vector component c stands for cos (and s for sin), m is the exponent of r, n is the frequency and 00 refers to the problem solution. Using this notation, the solution to problem (E_{00}) with $\kappa_\Delta = 0$ writes

$$u_{00}^{r30} = -\frac{(3-\nu)}{64}(\kappa_\Sigma^2 - \kappa_\Delta^2) \tag{A37}$$

$$u_{00}^{r10} = \frac{(R(\kappa_\Sigma^2 - \kappa_\Delta^2))^2}{64}(1-\nu) \tag{A38}$$

Therefore, its strain tensor writes

$$\underline{\underline{\epsilon}}_{00}(r) = \left(\frac{\kappa_\Sigma^2 - \kappa_\Delta^2}{64}\right)\begin{bmatrix} (1-\nu)R^2 - (3\nu-1)r^2 & 0 \\ 0 & (1-\nu)R^2 - (3-\nu)r^2 \end{bmatrix} \tag{A39}$$

This solution may then be used in Equation (11) to find the corresponding stress tensor.

A.1.4 | Solution to problem (E_{10})

The solution to problem (E_{10}) writes

$$u_{10}^{r30} = -\frac{1+\nu}{128}(\kappa_\Sigma^2 - \kappa_\Delta^2) \tag{A40}$$

$$u_{10}^{r10} = \frac{1+\nu}{128}(\kappa_\Sigma^2 - \kappa_\Delta^2)R_0^2 \tag{A41}$$

for the terms with a frequency $n=0$. Then, an inhomogeneous term with $n=1$ and $m=4$ is expected (due to the u_{00}^{r10} coefficient, which is not nil). From the equilibrium equation, one can find that its coefficients must verify the equation:

$$\begin{bmatrix} 8\nu-8 & 0 & 0 & 4\nu-4 \\ 0 & 8\nu-8 & 4\nu-4 & 0 \\ 0 & 8 & -16 & 0 \\ -8 & 0 & 0 & -16 \end{bmatrix} \cdot \begin{bmatrix} u_{10}^{rc14} \\ u_{10}^{rs14} \\ u_{10}^{\theta c14} \\ u_{10}^{\theta s14} \end{bmatrix} = -\begin{bmatrix} 1 & 0 & -1 & 0 & 0 & 0 \\ 0 & 0 & 0 & 0 & -2 & 0 \\ 0 & 0 & 0 & 0 & -2 & 0 \\ -1 & 0 & 1 & 0 & 0 & 0 \end{bmatrix} \cdot \begin{bmatrix} u_{00}^{r10} \\ 0 \\ u_{00}^{r10} \\ 0 \\ 0 \\ 0 \end{bmatrix} \tag{A42}$$

The second member is nil, and therefore, its coefficients are nil as well. Finally, two terms are expected for $n=4$, $m=n\pm1$. However, after tedious computation based on the equilibrium and boundary condition, one can find that the coefficients of the term $n=4$, $m=5$ are nil. The remaining term with $n=4$ and $m=3$ writes

$$\begin{bmatrix} u_{10}^{rc34} \\ u_{10}^{rs34} \\ u_{10}^{\theta c34} \\ u_{10}^{\theta s34} \end{bmatrix} = \left(\frac{1+\nu}{1-\nu}\right)\frac{\left(\kappa_\Sigma^2-\kappa_\Delta^2\right)}{192}\begin{bmatrix} 1 \\ 0 \\ 0 \\ -1 \end{bmatrix} \tag{A43}$$

Therefore, the strain tensor of problem (E_{10}) writes

$$\begin{aligned} \underline{\underline{\epsilon}}_{10}(r,\theta) &= (1+\nu)\left(\frac{\kappa_\Sigma^2-\kappa_\Delta^2}{64}\right)\left(\frac{1}{2}\begin{bmatrix} R_0^2-3r^2 & 0 \\ 0 & R_0^2-r^2 \end{bmatrix}\right. \\ &\left. +\left(\frac{1}{1-\nu}\right)r^2\left[\cos(4\theta)-\sin(4\theta)-\sin(4\theta)-\cos(4\theta)\right]\right) \end{aligned} \tag{A44}$$

A.1.5 | Solution to problem (E_{01})

The solution to this problem (E_{01}) will only contain terms of frequency $n>0$. For each frequency two homogeneous solutions with $r^{n\pm1}$ exist. Using the equilibrium and boundary conditions of problem (E_{01}), one can derive the following system that the coefficient of such terms must verify

$$\begin{bmatrix} f_1 & f_1 & 0 & 0 \\ 0 & 0 & f_2 & f_3 \\ g_1 & g_2 & g_5 & g_6 \\ -g_3 & g_4 & -g_7 & g_7 \end{bmatrix} \cdot \begin{bmatrix} u_{01}^{rcn-1n} \\ u_{01}^{\theta sn-1n} \\ u_{01}^{rcn+1n} \\ u_{01}^{\theta sn+1n} \end{bmatrix} = \frac{c_n}{c_4}\left(\frac{\left(\kappa_\Sigma^2-\kappa_\Delta^2\right)R_0^2}{32}\right)(1-\nu^2)\begin{bmatrix} 0 \\ 0 \\ 1 \\ n \end{bmatrix} \tag{A45}$$

with $f_1=(\nu+1)n^2/2-2n$, $f_2=(\nu+1)n^2/2+2n$, $f_3=n^2(1+\nu)/2+n(\nu-1)$, $g_1=(n-1+\nu)R^{n-2}$, $g_2=n\nu R^{n-2}$, $g_3=n(1-\nu)R^{n-2}/2$, $g_4=(n-2)(1-\nu)R^{n-2}/2$, $g_5=(n+1-\nu)R^n$, $g_6=n\nu R^n$, $g_7=n(1-\nu)R^n/2$. The four missing coefficients are nil. Please note that in this particular case, no explicit solution has been found. However, a numerical solution may be found for each frequency n and for a given set of parameters. After its computation, the strain tensor writes

$$\begin{aligned} \underline{\underline{\epsilon}}_{01}(r,\theta) = \sum_{n>0} r^{n-2}&\begin{bmatrix} (n-1)\cos(n\theta)u_{01}^{rcn-1n} & \frac{1}{2}\left((n-2)u_{01}^{\theta sn-1n}-nu_{01}^{rcn-1n}\right)\sin(n\theta) \\ \frac{1}{2}\left((n-2)u_{01}^{\theta sn-1n}-nu_{01}^{rcn-1n}\right)\sin(n\theta) & \left(nu_{01}^{\theta sn-1n}+u_{01}^{rcn-1n}\right)\cos(n\theta) \end{bmatrix} \\ +r^n&\begin{bmatrix} (n+1)\cos(n\theta)u_{01}^{rcn-1n} & \frac{n}{2}\left(u_{01}^{\theta sn-1n}-u_{01}^{rcn-1n}\right)\sin(n\theta) \\ \frac{1}{2}\left((n-2)u_{01}^{\theta sn-1n}-nu_{01}^{rcn-1n}\right)\sin(n\theta) & \left(nu_{01}^{\theta sn-1n}+u_{01}^{rcn-1n}\right)\cos(n\theta) \end{bmatrix} \end{aligned} \tag{A46}$$

In this form, the solution can easily be adapted for other values of c_n, that is, other geometries that correspond to a weakly perturbated disks.

A.1.6 | Solution for a thin strip

A flat rectangular strip of half length L_x and half width L_y is considered. This strip is conformed to a curved surface, and this conformation is modeled with a normal displacement $u_z\underline{e}_z$ such as described in Section 2.1. As L_y tends to be nil, it is assumed that there is an area where the strain field does not depend on x. One can compute the local variation in length of a small piece of matter along the x axis (see Figure 4A). At a given position y, the strip length is

$$dl(y)=\left(\frac{1}{\kappa_x}-\frac{1}{2}y^2\kappa_y\right)d\phi \tag{A47}$$

with κ_x and κ_y the curvatures along x and y and ϕ the angle presented on Figure 4A. This length variation corresponds to the existence of a varying ϵ_{xx} strain. Such a strain can be computed as: $dl(y)/dl(0)-1$. Since the choice of $dl(0)$ as the reference length is arbitrary, this result is valid to a constant.

$$\underline{\underline{\epsilon}}(y)=\begin{bmatrix} -\frac{1}{2}y^2\kappa_x\kappa_y+A & \epsilon_{xy}(y) \\ \epsilon_{xy}(y) & \epsilon_{yy}(y) \end{bmatrix} \tag{A48}$$

With an elastic material the corresponding stress field writes

$$\underline{\underline{\sigma}}(y)=\frac{E}{1-\nu^2}\begin{bmatrix} -\frac{1}{2}y^2\kappa_x\kappa_y+A+\nu\epsilon_{yy}(y) & \left(\frac{1-\nu+2b}{2}\right)\epsilon_{xy}(y) \\ \left(\frac{1-\nu+2b}{2}\right)\epsilon_{xy}(y) & \nu\left(-\frac{1}{2}y^2\kappa_x\kappa_y+A\right)+\epsilon_{yy}(y) \end{bmatrix} \tag{A49}$$

At equilibrium, the divergence of this tensor is nil. The corresponding vector writes

$$\underline{\nabla}.\left(\underline{\underline{\sigma}}\right)(y)=\frac{E}{1-\nu^2}\begin{bmatrix}\left(\frac{1-\nu+2b}{2}\right)\frac{d\epsilon_{xy}}{dy}(y)\\ -\nu y\kappa_x\kappa_y+\frac{d\epsilon_{yy}}{dy}(y)\end{bmatrix}=\underline{0} \quad (A50)$$

As a consequence, the shear strain is constant, $\epsilon_{xy}=B$ and $\epsilon_{yy}=\nu\frac{1}{2}y^2\kappa_x\kappa_y+C$. Finally, the loading on the outer boundaries must be nil. This condition writes

$$\left(\underline{\underline{\sigma}}.\underline{e}_y\right)(y=L_y)=\begin{bmatrix}\left(\frac{1-\nu+2b}{2}\right)B\\ \nu A+C\end{bmatrix}=\underline{0} \quad (A51)$$

So $B=0$, there is no shear. Finally, the external in-plane loading applied to the system is nil. Therefore, the overall stress applied at a given x must be nil. This writes

$$\int_{-L_y}^{L_y}\underline{\underline{\sigma}}.\underline{e}_x dy=\frac{E}{1-\nu^2}\begin{bmatrix}-\left(\frac{1-\nu^2}{3}\right)L_y^3\kappa_x\kappa_y+2L_y(A+\nu C)\\ 0\end{bmatrix}=\underline{0} \quad (A52)$$

From the above equations, $A=L_y^2\kappa_x\kappa_y/6$ and $C=-\nu L_y^2\kappa_x\kappa_y/6$. Finally, using the notations, κ_Σ and κ_Δ. The strain tensor writes

$$\underline{\underline{\epsilon}}(y)=\frac{\kappa_\Sigma^2-\kappa_\Delta^2}{24}\begin{bmatrix}L_y^2-3y^2 & 0\\ 0 & \nu\left(3y^2-L_y^2\right)\end{bmatrix} \quad (A53)$$

This last expression provides a strain prediction in the bulk of thin curved strips at equilibrium.

A.1.7 | Equation of the case study shape

The curved module presented as a case study in Section 4 is described by an out-of-plane transformation. Namely, the out of Oxy plane component z writes

$$z=-0.1\left(1.2(y+0.4)^2-y+2(y+0.35)^3\right)-0.2(1+y)x^2 \quad (A54)$$

where the coordinates are in meters. The shape is described for $x\in[-0.75;0.75]$ and $y\in[-0.35;0.35]$.